K-N Interaction in the $I=0$ State at Low Energies*†

V. J. STENGER,‡ W. E. SLATER, D. H. STORK, AND H. K. TICHO
Department of Physics, University of California, Los Angeles, California

AND

G. GOLDHABER AND S. GOLDHABER
Physics Department and Lawrence Radiation Laboratory, University of California, Berkeley, California

(Received 7 January 1964)

The study of the $I=0$ K-N interaction at low energies using K^+-deuterium scattering has been extended on the experimental side by the inclusion of elastic and inelastic noncharge-exchange scattering, and on the theoretical side by a more detailed investigation of the final-state interaction between the two nucleons. The new results for the $I=0$ phase shifts exhibit the same trends as those published before; however, the new s-wave data are more accurate. It is shown that at very low energies, the $I=0$ s-wave scattering may be interpreted as due to a very small scattering length $A_0=+0.04\pm0.04$ F. This should be contrasted with the $I=1$ scattering length $A_1=-0.31\pm0.01$ F.

I. INTRODUCTION

THE present report describes the last of a series of studies of the K-N interaction at low energies based on data secured in an exposure of the Lawrence Radiation Laboratory (LRL) 15-in. bubble chamber, filled alternately with hydrogen and deuterium, to separated beams of positive kaons with momenta ranging from 810 MeV/c down to zero.

The results of the completed study of K^+-proton scattering have already been reported.[1] This study showed that the preliminary evidence derived from K^+-proton scattering in nuclear emulsion[2] and from early scintillation counter studies[3] was indeed correct. For incident momenta below 640 MeV/c, the K-N interaction in the $I=1$ state is due essentially to pure s-wave scattering. Moreover, the low-momentum data[1] showed clearly that the interference between the Coulomb and the nuclear interaction was constructive. This, too, confirmed the early emulsion studies[4–6] which demonstrated that the *mean* nuclear potential seen by K^+ mesons in interactions with complex nuclei was repulsive.

It was shown in Ref. 1 that up to 640 MeV/c, the $I=1$ s-wave phase shift,[7] $\delta_{10}{}^{1/2}$, may be thought of as arising from a repulsive core with a radius of 0.31 ± 0.01 F. Alternatively, using the finite-range approximation, such that $k\cot\delta_{10}{}^{1/2}=(1/A_1)+(r_0/2)k^2$, the data up to 810 MeV/c are well represented by $A_1=-0.29\pm0.015$ F, $r_0=0.5\pm0.15$ F.

At 810 MeV/c, the differential K^+-proton scattering cross section appears to show the first statistically significant departure from isotropy.[8] As may be seen by comparing these data with those at[9] 910 MeV/c and at[10] 970 MeV/c, this anisotropy increases rapidly with momentum and appears to be accompanied by a rapid rise of the pion-production cross section.[10] At 1970 MeV/c, the angular distribution already shows a pronounced diffraction peak.[10]

The K-N interaction in the $I=0$ state is known with much less certainty. In part, this is due to the fact that, to date, the $I=0$ K-N system has been investigated by studying the interactions of K^+ mesons with neutrons bound in nuclei. The specific K^+-neutron interaction must then be isolated from effects due to neutron binding. However, apart from this "experimental" difficulty, it also appears that the description of the low-energy K-N interaction in the $I=0$ state demands more parameters than the $I=1$ state. Even the earliest studies of inelastic scattering and charge exchange in emulsion[11,12] at $\sim$300 MeV/c suggested the need for

* Supported at University of California at Los Angeles in part by U. S. Atomic Energy Commission contract AT(11-1)-34, Project 89, and carried out under the auspices of the U. S. Atomic Energy Commission at Berkeley.

† Submitted in partial fulfillment of the requirements for the Ph.D. degree at University of California at Los Angeles by V. J. Stenger.

‡ Present address: Department of Physics, University of Hawaii, Honolulu, Hawaii.

[1] S. Goldhaber, W. Chinowsky, G. Goldhaber, W. Lee, T. O'Halloran *et al.*, Phys. Rev. Letters **9**, 135 (1962).

[2] For general review, see M. F. Kaplon, *Proceedings of the 1958 Annual International Conference on High Energy Physics, CERN*, edited by J. Prentki (CERN, Geneva, 1958); D. Keefe, A. Kernan, A. Montwill, M. Grilli, L. Guerriero, and G. A. Salandin, Nuovo Cimento **12**, 241 (1959). This paper also contains a review of work to 1958.

[3] T. F. Kycia, L. T. Kerth, and R. G. Baender, Phys. Rev. **118**, 553 (1960).

[4] G. Igo, D. G. Ravenhall, J. J. Tieman, W. W. Chupp, G. Goldhaber *et al.*, Phys. Rev. **109**, 2133 (1958); J. E. Lannutti, S. Goldhaber, G. Goldhaber, W. W. Chupp, S. Giambuzzi *et al.*, *ibid.* **109**, 2121 (1958).

[5] M. A. Melkanoff, O. R. Price, D. H. Stork, and H. K. Ticho, Phys. Rev. **113**, 1303 (1959).

[6] B. Sechi-Zorn and G. T. Zorn, Phys. Rev. **120**, 1898 (1960).

[7] The notation $\delta_{I,l}{}^J$, with I, the isotopic spin l, the orbital angular momentum, and J, the total angular momentum, is employed.

[8] T. F. Stubbs, H. Bradner, W. Chinowsky, G. Goldhaber, S. Goldhaber *et al.*, Phys. Rev. Letters **7**, 188 (1961).

[9] W. Hirsch and G. Gidal, Lawrence Radiation Laboratory Report, UCRL-10950 (unpublished).

[10] V. Cook, D. Keefe, L. T. Kerth, P. G. Murphy, W. A. Wenzel, and T. F. Zipf, Phys. Rev. **129**, 2743 (1963).

[11] O. R. Price, D. H. Stork, and H. K. Ticho, Phys. Rev. Letters **1**, 212 (1958); M. A. Melkanoff, D. J. Prowse, D. H. Stork, and H. K. Ticho, *ibid.* **5**, 108 (1960).

[12] M. Grilli, L. Guerriero, M. Merlin, and G. A. Salandin, Nuovo Cimento **10**, 205 (1958).

positive p-wave phase shifts of $\sim 15°$ in the $I=0$ state. When the incident momentum was increased from 300 to ~ 500 MeV/c the mean nuclear potential decreased[13] from 21 to 13 MeV and the percentage of charge exchange events[4,13] among all inelastic interactions increased from 17% to 45%. This, too, could be understood in terms of rising p-wave phase shifts.

One study of the K-N $I=0$ interaction based on the data of this experiment has already been reported.[14] In the bubble chamber charge-exchange events

$$K^+ + d \rightarrow K^0 + p + p, \qquad \text{(A)}$$

with subsequent K_1^0 decay into charged pions are easily detected and unambiguously identified. Accordingly, this study was based on the charge-exchange events observed when the deuterium-filled 15-in. bubble chamber was exposed to K^+ mesons with momenta of 812 ± 6, 642 ± 7, 530 ± 15, 377 ± 18, 330 ± 23, and 230 ± 40 MeV/c. The $I=0$ phase shifts were extracted from the K^+-deuterium interactions by invoking the impulse approximation.[15] To avoid the need to consider the interaction of the two protons in the final state, the closure approximation[16] was used as well. With these approximations, the charge-exchange data could not be fitted without invoking the presence of p waves and possibly also d waves in the $I=0$ state.[14] The behavior of the $I=0$ s-wave phase shift $\delta_{00}^{1/2}$ near zero energy remained undetermined in the analysis.

In two theoretical papers attempts were made to fit the charge exchange data of Ref. 14 *including* the effect of the final-state interaction between the two protons. According to Ferreira[17] the data could be fitted by s-wave parameters alone once the Coulomb interaction between the protons was included. Lévy-Leblond and Gourdin[18] required p and d waves in $I=0$ even when final-state interactions were included. Both papers disagreed with the conclusions of Ref. 14 and of the present report.

The investigation of the K-N $I=0$ interaction has been continued in order to explore how the earlier results[14] might be improved. Section II describes the experimental procedure employed in the study of elastic scattering,

$$K^+ + d \rightarrow K^+ + d, \qquad \text{(B)}$$

and inelastic scattering[19]

$$K^+ + d \rightarrow K^+ + n + p. \qquad \text{(C)}$$

The interaction of the two nucleons in the final state is considered in Sec. III. In Sec. IV, the new elastic and inelastic scattering data are combined with the charge-exchange data of Ref. 14 and a new set of $I=0$ phase shifts is calculated. This calculation employs the new $T=1$ s-wave phase shift of Ref. 1 and does not use the closure approximation. The new $T=0$ phase shifts indicate less s-wave and more p-wave scattering than the earlier results.[14] The s-wave scattering in $I=0$ becomes very small as the incident momentum approaches zero but does not change sign. The new results and those of Ref. 14 show small systematic differences; the old and the new phase shifts agree within errors, however.

II. EXPERIMENTAL CONSIDERATIONS

The K^+ beam design[20] and many details of the experimental procedure have already been discussed.[1,14] This section deals only with those aspects which bear specifically on the measurement of the elastic and inelastic cross sections.[21] These cross sections were investigated at 230 ± 40, 377 ± 18, and 530 ± 15 MeV/c; at the higher momenta the experimental difficulties in identifying the outgoing particles became insurmountable. All the film used in the experiment was scanned at least twice and the over-all scanning efficiencies were $>99\%$.

In general, elastic and inelastic scatters, reactions (B) and (C), appear in the bubble chamber as two-prong events or as one-prong events if the deuteron or proton is not energetic enough. Both one- and two-prong events have a small background due to charge exchange events in which the K^0 does not decay into a charged pion pair in the chamber. The one-prong events also have a large background due to K-meson decays. In addition, there are background interactions produced by incident pions from K^+ decay ahead of the chamber and by incident protons. The latter result from K^+ interactions in the tungsten absorbers placed into the beam in front of the chamber to reduce the beam momentum from the design value of 642 MeV/c to the value desired in the run. After these background events are suppressed, there still remains the problem of separating the elastic events from the inelastic ones.

The aims and procedures of the 230 MeV/c study and of those at the two higher momenta differed in some respects and will be discussed separately.

---

[13] D. Evans, F. Hassan, K. K. Nagpaul, M. Shafi, E. Helmy, J. H. Mulvey, D. J. Prowse, and D. H. Stork, Nuovo Cimento **10**, 168 (1958).

[14] W. E. Slater, D. H. Stork, H. K. Ticho, W. Lee, W. Chinowsky *et al.*, Phys. Rev. Letters **7**, 378 (1961). For details, see W. Lee, thesis, 1961 (unpublished); Lawrence Radiation Laboratory Report UCRL-9691 (unpublished).

[15] G. Chew, Phys. Rev. **80**, 196 (1950); S. Fernbach, T. Green, and K. Watson, *ibid.* **84**, 1084 (1951); R. Rockmore, *ibid.* **105**, 256 (1957).

[16] E. Ferreira, Phys. Rev. **115**, 1727 (1959).

[17] E. Ferreira, thesis, University of London, 1961 (unpublished); Notas de Fisica **8**, 4 (1961).

[18] J. M. Lévy-Leblond and M. Gourdin, Nuovo Cimento **23**, 1163 (1962).

[19] While both (A) and (C) represent inelastic processes, of course, (A) will be referred to as charge exchange and (C) as inelastic scattering.

[20] G. Goldhaber, S. Goldhaber, T. Kadyk, T. Stubbs, D. H. Stork, and H. K. Ticho, University of California, LRL Internal Report, Bev 483, 1960 (unpublished).

[21] For details, see V. J. Stenger, thesis, UCLA, 1963 (unpublished).

A. The 230 MeV/c Data

At 230 MeV/c, the elimination of the backgrounds was relatively easy. First of all, in $\sim 70\%$ of the interactions the scattered kaon stopped and decayed within the chamber. Charge-exchange events were rare and both protons almost always stopped in the chamber. Most K^+ decays were eliminated on inspection because of the great change of bubble density between the K^+ and the decay particle. The great majority of incident protons were rejected by the angular beam entrance criteria. The fiducial volume was chosen small enough such that, even if they did not stop in the chamber, the scattered kaons could be separated by curvature and ionization from scattered protons and from slow decay pions and muons. To avoid scanning losses, only events with scattering angle θ_{lab} satisfying $-1.0 \leqslant \cos\theta_{\text{lab}} \leqslant +0.95$ were recorded. Subject to these criteria, 546 elastic and inelastic scattering events were found. In the same film, 211 τ decays were found using the same criteria of entrance and fiducial volume. The momentum distribution of these τ decays obtained by kinematic fitting of the decay vertices is shown in Fig. 1. The wide momentum spread is a consequence of both straggling in the tungsten absorber and momentum loss in the chamber itself. The mean momentum was actually 206 MeV/c. In translating the τ count into kaon track length, a branching fraction of 5.7% was used.[22]

Although essentially all deuterons from elastic scatters and all protons from the inelastic events stopped in the chamber, it was in most cases impossible to distinguish these two processes. Except for the rare cases when the recoil particles could be identified as deuterons from range *and* curvature, all elastic events also fitted the inelastic process. The following method was used to determine the number of elastic events statistically. For each event with a recoil track longer than l_0, two parameters, $\cos\gamma$ and Δ, were computed; $\cos\gamma$ is the deviation from coplanarity and Δ the fractional deviation from transverse momentum balance. Here

$$\cos\gamma = \frac{\mathbf{d}}{|\mathbf{d}|}\cdot\frac{\mathbf{k}\times\mathbf{k}_0}{|\mathbf{k}\times\mathbf{k}_0|} \quad \text{and} \quad \Delta = \frac{|\mathbf{k}\times\mathbf{k}_0| - |\mathbf{d}\times\mathbf{k}_0|}{|\mathbf{k}\times\mathbf{k}_0| + |\mathbf{d}\times\mathbf{k}_0|}; \quad (1)$$

$\mathbf{k}_0$ and $\mathbf{k}$ are the initial and final momentum vectors of the kaon, respectively, and $\mathbf{d}$ is the momentum of the recoil particle computed from its range *assuming* that it was a deuteron. Figure 2 shows the scatter plot for events with $l_0 = 0.5$ cm. Elastic events are expected to lie within experimental errors of the origin. Inelastic events in which the kaon collides with the proton while the neutron acts as spectator should show a distribution in $\cos\gamma$ which peaks at zero and a Δ distribution which peaks at -0.23. This is due to the fact that, when the proton is assumed to be a deuteron, its momentum from range is overestimated by a factor of ~ 1.6. Finally, for scatters on neutrons the $\cos\gamma$ distribution of the spectator protons should be flat. Figure 2 may be interpreted as a superposition of these three processes.

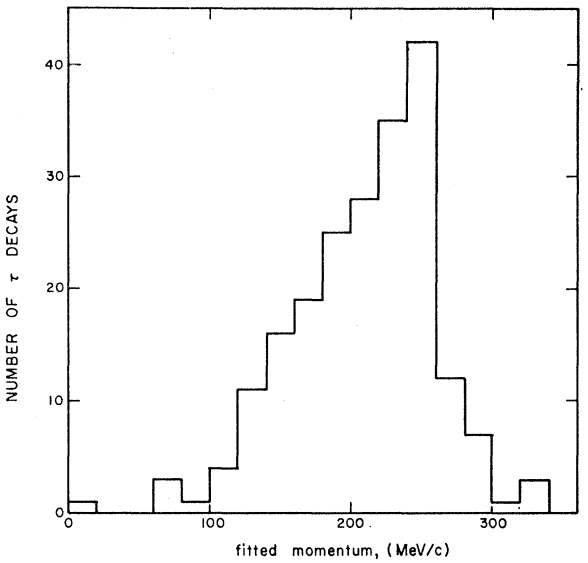

FIG. 1. Momentum spectrum of fitted τ decays in the film with 230-MeV/c nominal beam momentum.

Events were called elastic if they fell within $|\cos\gamma| \leqslant 0.1$ and $|\Delta| \leqslant 0.10$ for stopping K^+, $|\Delta| \leqslant 0.15$ for K^+ which left the chamber. The background was estimated by interpolation using the number of events just outside the "elastic" region. Table I gives the number of elastic events for various values of l_0.

B. The 377 and 530 MeV/c Data

At 230 MeV/c, the fraction of identifiable elastic scatters among all noncharge-exchange events was $\sim 20\%$. At the higher momenta, the number of elastic scatters was expected to be small. Hence, no separation was attempted between the examples of reactions (B) and (C).

At these momenta, kinematic fitting alone turned out to be of little use in separating the interactions from the backgrounds. This is illustrated in Fig. 3(a),

TABLE I. Number of events with $-1.0 \leqslant \cos\theta_{\text{lab}} \leqslant 0.95$ classified as "elastic" for various lengths $l \geqslant l_0$ of the recoil particle. $N_{\text{total}} = 546$.

l_0 (cm)	$N_{\text{el}}(l \geqslant l_0)$	$N_{\text{inel}} + N_{\text{el}}(l < l_0)$
0.50	110	436
0.85	92	454
1.20	61	485

[22] B. P. Roe, D. Sinclair, J. L. Brown, D. A. Glaser, J. A. Kadyk, and G. H. Trilling, Phys. Rev. Letters 7, 346 (1961).

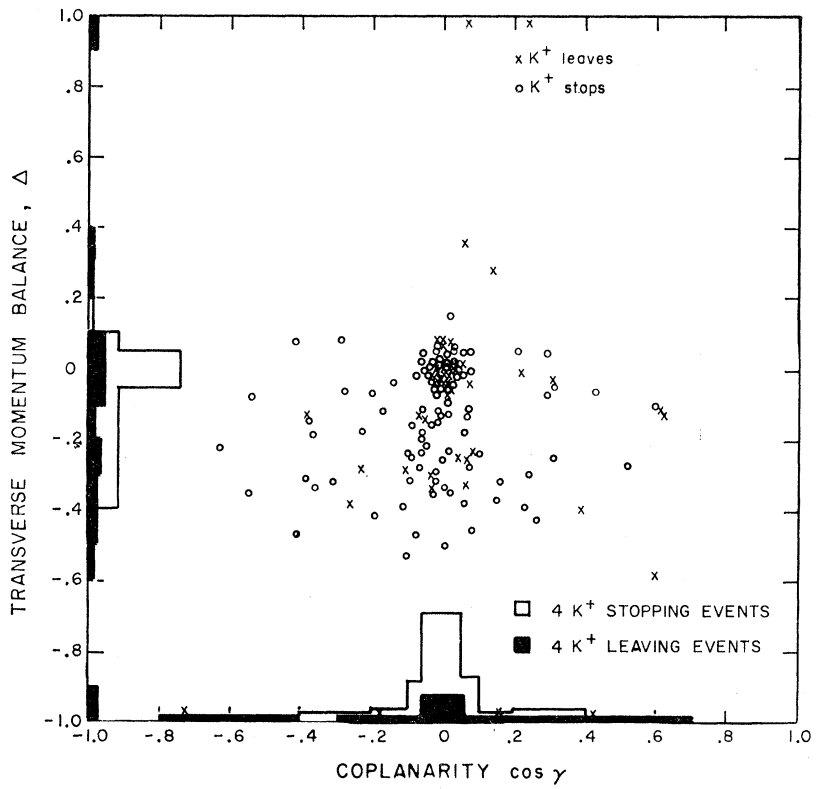

FIG. 2. Scatter plot of coplanarity and transverse momentum balance for the 230-MeV/c data with $l_0=0.50$ cm.

which is applicable to the one-prong events initiated by 377-MeV/c kaons. Figure 3(a) shows, first of all, the momenta of π's and μ's from $K_{\pi 2}$ and $K_{\mu 2}$ decays, respectively, plotted versus laboratory angle of emission. Also shown are the bands of momenta for the scattered K^+ due to reaction (C) and for the recoil proton in reaction (A) (labeled PR). The widths of the bands were established by the consideration that, in order for an event to appear one-pronged, the spectator proton must have a range too short to be visible and therefore a momentum $\lesssim$100 MeV/c. The impulse approximation then implies that the neutron which participated in the interaction also has a momentum of $\lesssim$100 MeV/c. The boundaries of the bands are the extremes for collisions on 100-MeV/c neutrons moving in arbitrary directions.

The essential point illustrated by Fig. 3(a) is that in the laboratory, beyond $\sim$30°, decay, inelastic scattering, and charge exchange cannot be separated without ionization measurements. The same applies to the separation of two-prong events into scattering and charge exchange. The expected track opacity for the various processes is shown in Fig. 3(b). The I scale used as ordinate is related to the ionization as described in the next paragraph.

A quantity I monotonically related to the ionization along the track was determined by projecting onto the image of the track a bright image of a slit whose width, position, curvature, and finally brightness were adjusted until the track just disappeared into the background. The iris opening of the lens used to project the slit served as ionization indicator. Because of variations in the chamber operating conditions, film development, etc., the quantity actually used was the ratio of lens openings for the secondary and the primary tracks. Corrections were applied to take into account the dip of the track and the variation of saturation with dip. However, to keep these corrections small, only those events were used where the angle ϕ between the camera image plane and the plane formed by the incident and the outgoing track was $<60°$. Figure 4 shows a calibration curve of the densitometer which was obtained using (mainly) tracks from fitted charge-exchange events with visible K^0 decay. The mean fractional spread in the determination of I is 9%.

At 377 and 530 MeV/c, the ionizations of the incident kaons are 2.5 and 1.7 times minimum, respectively. Thus it was possible to eliminate by inspection the great bulk of forward one-prong decays which produce minimum ionizing secondaries. At 640 MeV/c, this procedure was no longer possible as both secondary kaons and decay particles ionized near minimum.

Table II shows the numbers of events of types (B) and (C) combined found at the two momenta.

To avoid scanning biases, only events with scattering angles $\theta_{\rm lab}>5°$ were recorded. The angular distributions are shown in Figs. 10(a) and 11(a). Of the 365 events on which ionization measurements had to be carried

TABLE II. Elastic plus inelastic interactions found at 377 and 530 MeV/c. $\theta_{\text{lab}}>5°$. The numbers in parentheses are one-prong events.

Momentum (MeV/c)	Events examined	Kinematics	Resolved by K Decay	Ionization	Ambiguous	Total
377±18	3353	13 (11)	30 (8)	89 (6)	4 (0)	136±12
530±15	2149	6 (2)	16 (4)	107 (23)	4 (1)	133±12

out, 166 were backgrounds, 191 were K^+ scatters, and 8 remained ambiguous.

The kaon track lengths were determined by a count of beam tracks satisfying the angular and ionization criteria in every twentieth frame. The track lengths at 377 and 530 MeV/c were $(2.75\pm0.14)\times10^5$ and $(2.81\pm0.13)\times10^5$ cm, respectively. The corresponding cross sections for elastic plus inelastic interactions (but excluding charge exchange) with $\theta_{\text{lab}}>5°$ are 19.7±1.9 mb at 377 MeV/c and 18.9±1.8 mb at 530 MeV/c.

The method developed for the separation of the events also leads to the identification of charge-exchange events with *invisible* K^0 decay; 19 such events were found at 377 MeV/c and 34 at 530 MeV/c. These yield charge-exchange cross sections of 4.2±1.2 mb and 7.2±1.5 mb, respectively. These cross sections are in good agreement with 3.1±0.4 and 6.5±0.6 mb, respectively, observed[14] at these two momenta using charge-exchange events *with* visible K^0 decay.

III. THEORY OF K^+-DEUTERIUM SCATTERING

Below the threshold for pion production, the three processes whereby K^+ mesons interact with nucleons and the corresponding scattering amplitudes are

$$K^++p\rightarrow K^++p, \quad (f_1+f_c), \tag{D}$$

$$K^++n\rightarrow K^++n, \quad \tfrac{1}{2}(f_1+f_0), \tag{E}$$

$$K^++n\rightarrow K^0+p, \quad \tfrac{1}{2}(f_1-f_0). \tag{F}$$

Since the processes represent scattering of a spin-zero particle by one of spin $\frac{1}{2}$, the scattering amplitude f_I is given by

$$f_I=a_I+\boldsymbol{\sigma}\cdot\hat{n}b_I, \tag{2}$$

where $\hat{n}$ is the normal to the scattering plane and a_I and b_I are the nonspin-flip and spin-flip amplitudes, respectively. These may be expanded

$$a_I=\sum_{l=0}^{\infty}\{(l+1)\eta_{Il}{}^{l+\frac{1}{2}}+l\eta_{Il}{}^{l-\frac{1}{2}}\}P_l{}^0(\cos\theta^*), \tag{3a}$$

$$b_I=-i\sum_{l=1}^{\infty}\{\eta_{Il}{}^{l+\frac{1}{2}}-\eta_{Il}{}^{l-\frac{1}{2}}\}P_l{}^1(\cos\theta^*), \tag{3b}$$

with

$$\eta_{Il}{}^J=(k^*)^{-1}\exp(i\delta_{Il}{}^J)\sin(\delta_{Il}{}^J). \tag{4}$$

k^* and θ^* are the c.m. momentum and scattering angle, respectively.

$$f_c=a_c=-\frac{\alpha}{2k^*\sin^2(\theta^*/2)}\exp\{-i\alpha\ln[\sin^2(\theta^*/2)]\} \tag{5}$$

is the Coulomb amplitude, $\alpha=1/(137v^*)$.

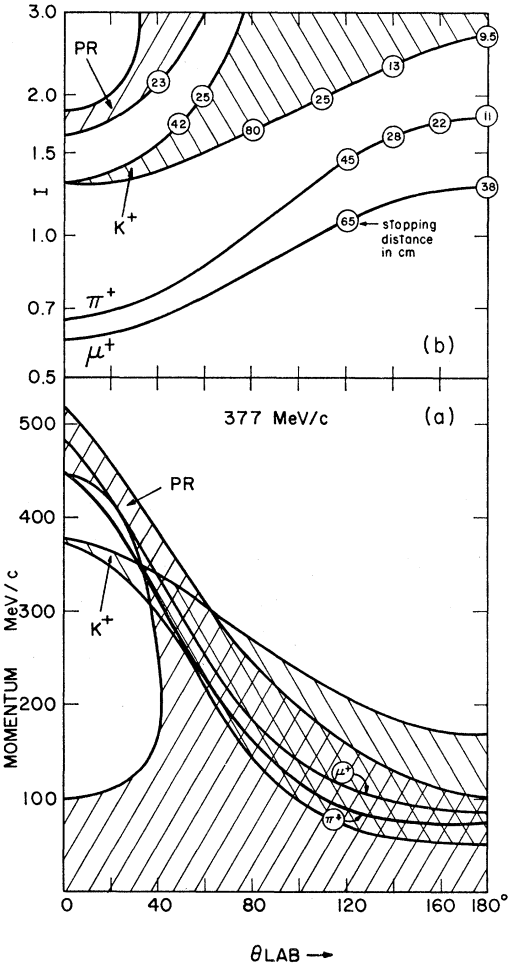

FIG. 3. Kinematics of the deflected particle in one-prong events at 377 MeV/c: (a) momentum versus deflection angle for $K_{\pi 2}$ and $K_{\mu 2}$ decays, K^+ scattering and proton recoil from charge exchange, (b) track opacity versus deflection angle for the same processes.

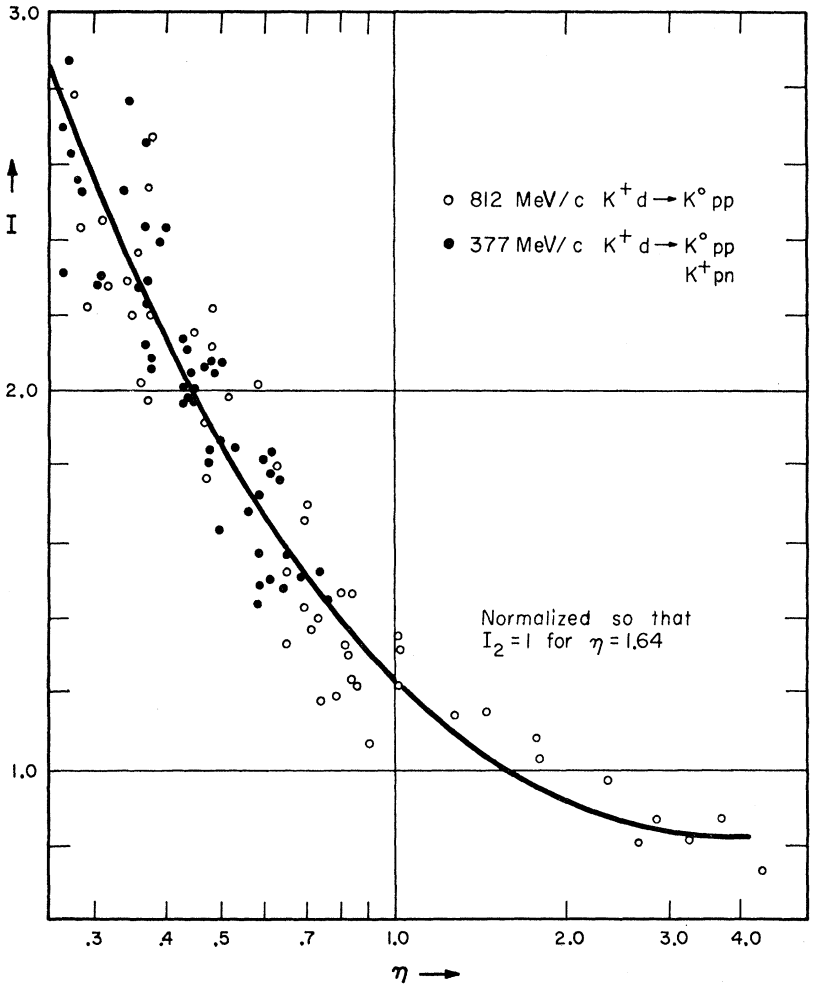

FIG. 4. Calibration curve of track densitometer. The beam track is used as standard.

Now, using the impulse approximation,[15–18,21,23,24] it is possible to express the cross sections for reactions (A), (B), and (C) in terms of the K-nucleon parameters a_I and b_I in a relatively simple way. Setting

$$a_p=a_1+a_c,\quad a_n=\tfrac{1}{2}(a_1+a_0),\quad a_e=\tfrac{1}{2}(a_1-a_0),\quad (6a)$$

$$b_p=b_1,\qquad b_n=\tfrac{1}{2}(b_1+b_0),\quad b_e=\tfrac{1}{2}(b_1-b_0),\quad (6b)$$

it is possible to show that

$$d\sigma^{\mathrm{CE}}/d\Omega^*=\{|a_e|^2+\tfrac{2}{3}|b_e|^2\}I_{ppt}+\tfrac{1}{3}\{|b_e|^2\}I_{pps},\quad (7)$$

$$d\sigma^{\mathrm{IN}}/d\Omega^*=\{|a_p|^2+|a_n|^2+\tfrac{2}{3}[|b_p|^2+|b_n|^2]\}I_{npt}+\tfrac{1}{3}\{|b_p|^2+|b_n|^2\}I_{nps}+2\,\mathrm{Re}\{a_n^*a_p+\tfrac{2}{3}b_n^*b_p\}J_{npt}-2\,\mathrm{Re}\{\tfrac{1}{3}b_n^*b_p\}J_{nps},\quad (8)$$

$$d\sigma^{\mathrm{EL}}/d\Omega^*=\{|a_p+a_n|^2+\tfrac{2}{3}|b_p+b_n|^2\}D.\quad (9)$$

The factors of $\frac{1}{3}$ arise from spin averages. The functions I, J, and D are deuteron form factors; e.g., I_{npt} means that the interaction leaves the nucleons in a proton-neutron charge state and the triplet spin state. The form factors are given by

$$I(k_0,\theta^{*\prime})=\frac{\omega(k')}{k'^2}\frac{dE_f'}{dk'}\int\frac{k^2dk}{\omega(k)}P^2\frac{dP}{dE_f}F(Q,P),\quad (10a)$$

$$J(k_0,\theta^{*\prime})=\frac{\omega(k')}{k'^2}\frac{dE_f'}{dk'}\int\frac{k^2dk}{\omega(k)}P^2\frac{dP}{dE_f}G(Q,P),\quad (10b)$$

where $\mathbf{P}$ is the relative momentum of the two nucleons in the final state and $\mathbf{Q}=\frac{1}{2}(\mathbf{k}_0-\mathbf{k})$. The vectors $\mathbf{k}_0$ and $\mathbf{k}$ are, respectively, the initial and final kaon momenta in the laboratory, $\omega(k)=(k^2+m_K^2)^{1/2}$, and E_f is the total energy in the final state in the laboratory. The primed quantities are those which would be inferred *from* the laboratory *scattering angle* under the assumption that the scattering took place on a stationary nucleon.[21] The quantity ahead of the integral contains the essential factors for a transformation from the laboratory scattering angle θ to a fictitious c.m. co-

[23] M. Gourdin and A. Martin, Nuovo Cimento **11**, 670 (1959).
[24] M. Gourdin and A. Martin, Nuovo Cimento **14**, 722 (1959).

TABLE III. The mean ratio $\langle\epsilon\rangle$ between the K-N momenta after the collision and before.

p(MeV/c)	$\langle\epsilon\rangle$
377	0.93
530	0.95
642	0.96

ordinate system in which the target nucleon is at rest. The functions F and G will be defined below.

Expressions (7) and (8) involve the true c.m. scattering angle θ^* (nucleon in motion) in a_I and b_I and the fictitious $\theta^{*\prime}$ (nucleon assumed at rest) in I and J. Figure 5 shows a scatter plot of $\cos\theta^*$ versus $\cos\theta^{*\prime}$ using charge events in which the K^0 decayed visibly[14];

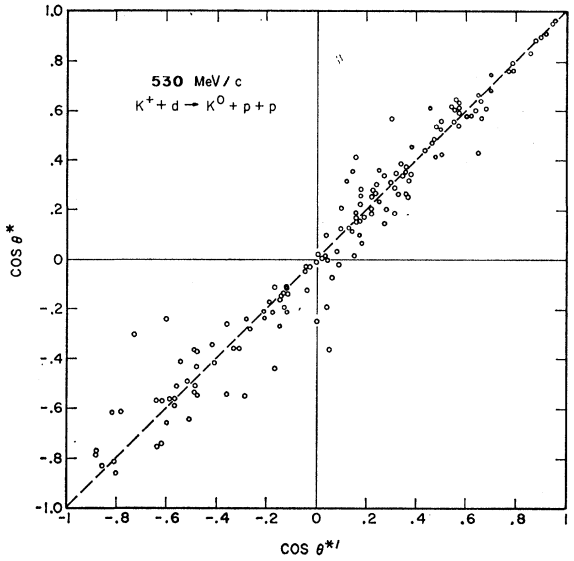

FIG. 5. Scatter plot of $\cos\theta^{*\prime}$, the c.m. scattering angle inferred from the laboratory scattering angle under the assumption that the target nucleon was at rest versus $\cos\theta^*$, the actual c.m. scattering angle obtained assuming that the momentum of the target nucleon was opposite to that of the spectator.

$\cos\theta^*$ was obtained by assuming that in each event the slower proton was the spectator and that the neutron on which the charge exchange took place had a momentum equal and opposite to that of the spectator proton. The rms difference between $\cos\theta^*$ and $\cos\theta^{*\prime}$ is 0.11. However, the deviations do not appear to exhibit a systematic trend, and therefore the effect of using $\cos\theta^*$ or $\cos\theta^{*\prime}$ on the differential cross sections is likely to be negligible. Accordingly, in what is to follow, no distinction will be made between θ^* and $\theta^{*\prime}$.

Since the deuteron binding energy and the energy of the spectator proton must be supplied by the incident kaon, the scattering amplitudes as determined by the impulse approximation are not on the energy shell. Again using the charge exchanges with visible K^0 decay[14] and defining the lower momentum proton to be the spectator, one can estimate the ratio ϵ between the K-N c.m. momenta after and before the collision. Table III gives $\langle\epsilon\rangle$ for three incident K^+ momenta.

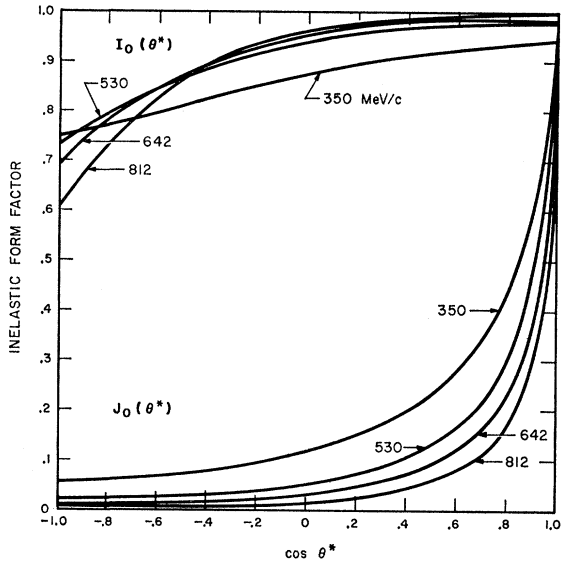

FIG. 6. The form factors $I_0(k_0, \cos\theta^*)$ and $J_0(k_0, \cos\theta^*)$ for $k_0=350$, 530, 642, and 812 MeV/c.

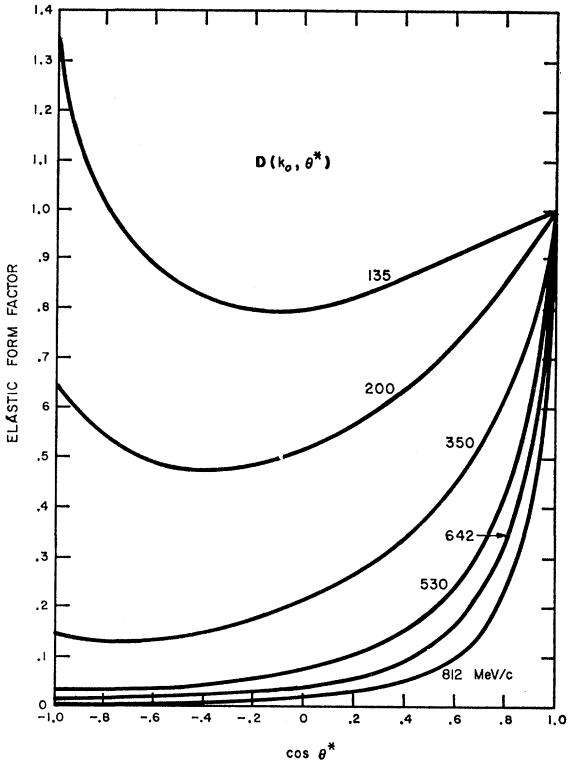

FIG. 7. The form factor $D(k_0, \cos\theta^*)$ for $k_0=135$, 200, 350, 530, 642, and 812 MeV/c. θ^* is *not* the K-d c.m. scattering angle but the c.m. angle which would have been computed from the *laboratory* scattering angle *if* the scattering had taken place on a *free* single nucleon.

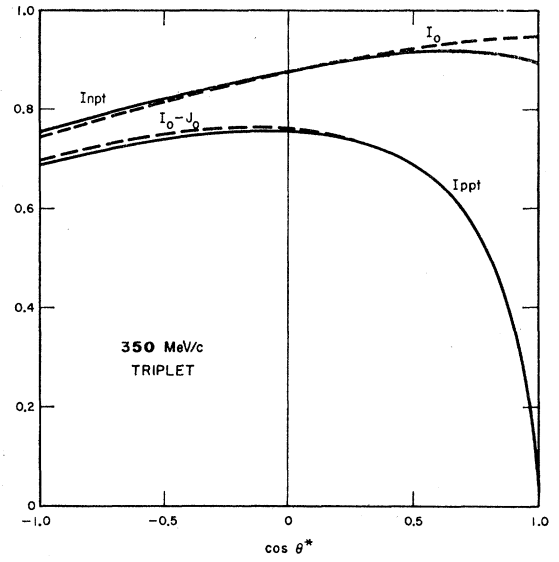

FIG. 8. Effect of nuclear phase shifts on the triplet form factors. The "exponential cutoff model" was used in the calculation.

The functions F and G in (10) are defined by

$$F(Q,P)=\int d\Omega_P\left|\int d^3r\Psi_P^*(\mathbf{r})\exp(i\mathbf{Q}\cdot\mathbf{r})\Psi_D(\mathbf{r})\right|^2, \quad (11)$$

$$G(Q,P)=\int d\Omega_P\int d^3r\Psi_P^*(\mathbf{r})\exp(i\mathbf{Q}\cdot\mathbf{r})\Psi_D(\mathbf{r})$$
$$\times\int d^3r'\Psi_P(\mathbf{r}')\exp(-i\mathbf{Q}\cdot\mathbf{r}')\Psi_D(\mathbf{r}'). \quad (12)$$

Ψ_D is the deuteron wave function and Ψ_P is the wave function of the two outgoing nucleons with relative momentum $\mathbf{P}$. For elastic scattering

$$D(k_0,\theta^*)=\frac{1}{k'^2}\frac{dE_f'}{dk'}k^2\frac{dk}{dE_f}|H_2(Q)|^2, \quad (13)$$

$$H_2(Q)=\int d^3r|\Psi_D(\mathbf{r})|^2\exp(i\mathbf{Q}\cdot\mathbf{r}). \quad (14)$$

In the following calculation, the Hulthén function

$$\Psi_D(r)=(N/r)(e^{-\alpha r}-e^{-\beta r});$$
$$N^2=[\alpha\beta(\alpha+\beta)/2\pi(\beta-\alpha)^2], \quad (15)$$

with $\alpha=45.7$ MeV, $\beta=7\alpha$ was used. If the final-state wave function is taken to be a plane wave, then integrals (11) and (12) can be solved analytically.[23,24] The expressions are given in the Appendix. In the plane-wave approximation, the six form factors reduce as follows:

$$I_{npt}\rightarrow I_0,\quad I_{nps}\rightarrow I_0,\quad J_{npt}\rightarrow J_0,\quad J_{nps}\rightarrow J_0,$$
$$I_{ppt}\rightarrow I_0-J_0,\quad I_{pps}\rightarrow I_0+J_0. \quad (16)$$

The integrations (10) required to determine I_0 and J_0 have been computed on an IBM-7090 computer. They are shown in Fig. 6. Figure 7 shows the behavior of the elastic form factor[25] $D(k_0,\theta^*)$.

One of the motivations of this study was to determine whether the anisotropic charge exchange angular distribution on deuterium given in Ref. 14 and shown again in Figs. 10, 11, and 12 could be due to final-state interactions of the two protons while the elementary K-N $I=0$ and $I=1$ interactions *both* involved only s waves. For s-wave interaction only $b_p=b_n=b_e=0$ and only the first term in Eq. (7) is retained. Two protons in a triplet state must be in a state of odd-orbital angular momentum L.

The effect of the Coulomb interaction in the $L=1$ channel was calculated by inserting Coulomb wave functions into (10) and (11). The Coulomb wave function differs appreciably from the plane wave only at relative momenta $P<10$ MeV/c. Because of the size of the deuteron, these momenta contribute negligibly to the integrals. Hence, the Coulomb interaction appears to be negligible in the $L=1$ channel and, *a fortiori*, for $L>1$.

In contrast to the Coulomb effect, the proton-proton nuclear phase shifts are large at the momenta which contribute strongly to the integrals (10). However, the wave function is poorly known within the interaction region. One can avoid this region by the use of the "boundary condition model"[26] where the two-nucleon radial wave function is written

$$W_L{}^J(Pr)=j_L(Pr)\cos\delta_L{}^J-n_L(Pr)\sin\delta_L{}^J, \quad r>r_c$$
$$=0, \quad r<r_c. \quad (17)$$

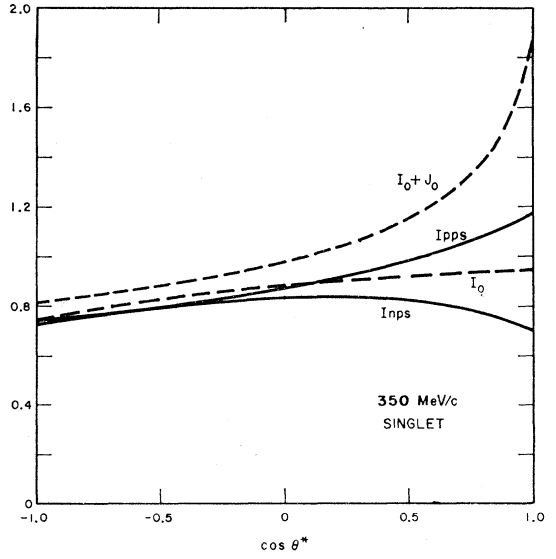

FIG. 9. Effect of nuclear phase shifts on the singlet form factors. The "momentum-dependent cutoff model" was used in the calculation.

[25] See the caption on Fig. 7 for definition of θ^* in this case.

[26] D. P. Saylor, R. A. Bryan, and R. E. Marshak, Phys. Rev. Letters **5**, 266 (1960).

The I_{ppt} form factor calculated using (17) and the published proton-proton phase shifts[27] was found to depend strongly[21] on r_c. This sensitivity disappeared when an exponential cutoff[24] was used, such that

$$W_L{}^J(Pr)=j_L(Pr)\cos\delta_L{}^J-n_L(Pr) \times\sin\delta_L{}^J(1-e^{-r/r_c})^{L+1}. \quad (18)$$

I_{ppt} and I_{npt}, calculated using (18) with $k_0=350$ MeV/c are shown in Fig. 8. The deviations from the plane-wave form factors are small.

The singlet form factors obtained using a *momentum-dependent* cutoff factor $r_c=r_c'P$ are shown in Fig. 9. The marked effect of the nuclear interaction at forward scattering angles is due primarily to the strong singlet $L=0$ interaction. However, as may be seen from Eqs.

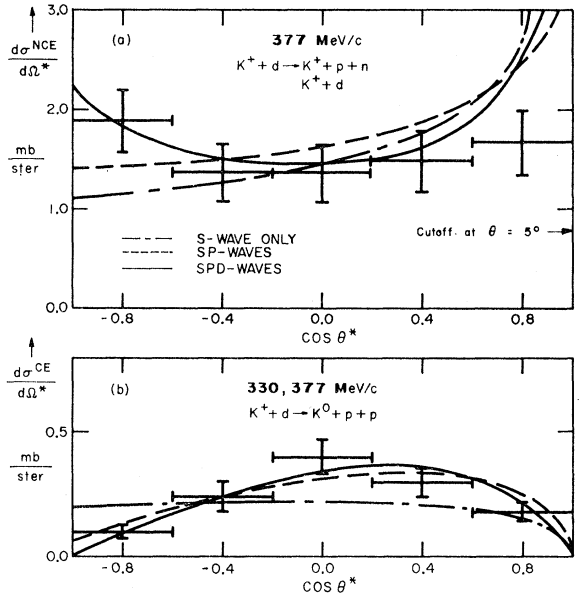

FIG. 10. (a) The noncharge-exchange angular distribution at 377 MeV/c. (b) The charge-exchange (Ref. 14) data at 330 and 377 MeV/c combined. The smooth curves are fits as given in Tables IV and V.

(7) and (8), the singlet form factors multiply the spin-flip terms and these vanish for $\cos\theta^*=1$. Hence the effect of the nuclear interactions is small in the singlet state as well.

Since the cutoff procedures described above are admittedly somewhat arbitrary, the triplet p-p wave function inside the range of nuclear forces was also calculated according to the Bryan-Dismukes-Ramsay model.[28] The deviation from the plane-wave result of

[27] M. H. MacGregor, M. J. Moravcsik, and H. P. Stapp, Lawrence Radiation Laboratory Report UCRL 6082 (unpublished). M. H. Hull, K. E. Lassila, H. M. Ruppel, F. A. McDonald, and G. Breit, Phys. Rev. **122**, 1606 (1961).

[28] R. A. Bryan, C. R. Dismukes, and W. Ramsay (to be published). We are grateful to these authors for making their computer code available to us.

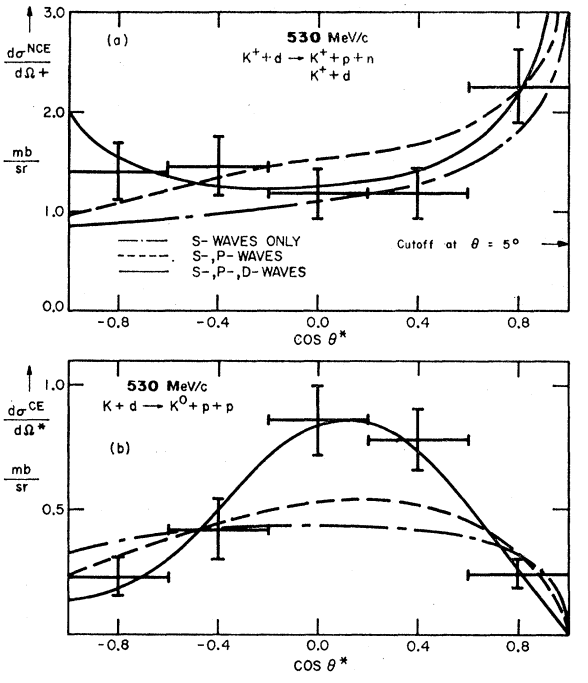

FIG. 11. The 530-MeV/c data (a) noncharge-exchange data, (b) charge-exchange angular distribution (Ref. 14). The smooth curves are fits as given in Tables IV and V.

I_{ppt} calculated using the BDR model was somewhat smaller than the deviation found using the exponential cutoff model. It appears likely therefore that the effect of the nucleon-nucleon phase shifts on the form factors is somewhat smaller than that suggested by Figs. 8

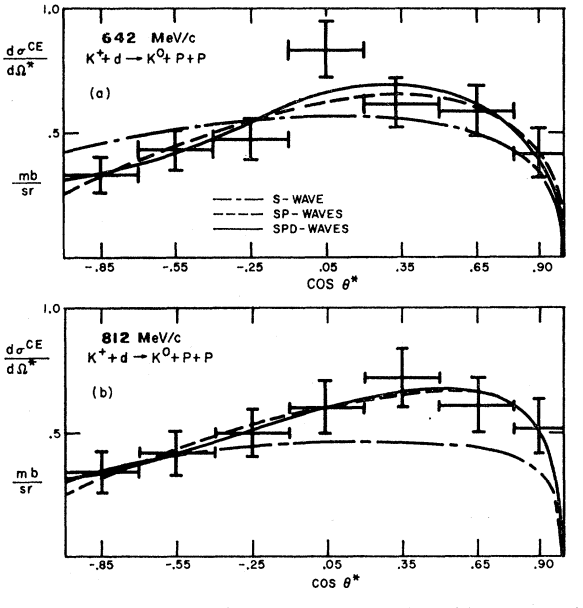

FIG. 12. The charge-exchange data (Ref. 14) at (a) 642 MeV/c and (b) 812 MeV/c. The smooth curves are fits as given in Tables IV and V.

TABLE IV. *SP* solutions to phase-shift analysis. Subscripts 1, 2, 3 correspond to $\delta_{00}^{1/2}$, $\delta_{01}^{1/2}$, $\delta_{01}^{3/2}$.

k_0 MeV/c	$\delta_{10}^{1/2}$ deg.	$\delta_{00}^{1/2}$ deg.	$\delta_{01}^{1/2}$ deg.	$\delta_{01}^{3/2}$ deg.	Correlation coefficients C_{12}	C_{13}	C_{23}	χ^2	No. of const.	$P(\chi^2)$
350 (1.12 F^{-1})	−20.0	3.8±1.2	2.5±14.9 3.2±15.2	3.1±7.6 2.7±7.5	0.28 −0.27	−0.30 0.25	−0.99 −0.99	25.6	7	<0.01
530 (1.60 F^{-1})	−29.4	6.3±4.1	−17.2±3.3 23.0±4.1	12.3±2.8 −6.5±4.9	0.47 −0.74	−0.74 0.01	−0.52 −0.12	22.9	7	<0.01
642 (1.88 F^{-1})	−36.2	15.1±18.8	−18.8±7.3 29.8±21.2	16.8±12.3 −5.0±2.8	0.91 −0.98	−0.98 −0.75	−0.90 0.76	4.4	4	0.43
812 (2.26 F^{-1})	−47.0	18.0±14.4	−18.2±5.8 39.4±16.3	24.0±9.2 −2.1±8.6	−0.67 0.94	−0.92 −0.94	0.69 0.93	0.7	4	0.95

and 9. The plane-wave form factors thus appear adequate and are used in the determination of the $I=0$ K-N phase shifts.

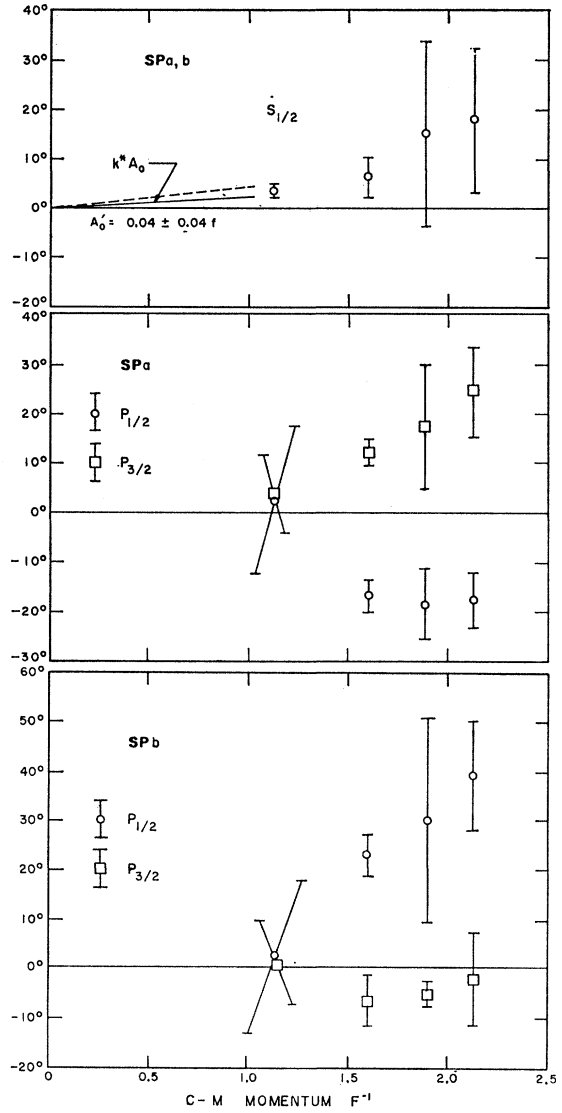

FIG. 13. The $I=0$ phase shifts of Table IV plotted versus momentum. The *a* and *b* solutions are the Fermi-Yang ambiguity. The low-energy behavior of the *s* wave, as specified by the $I=0$ scattering length A_0, is also shown. The solid line refers to $A_0=+0.04$ F, the dotted line to $A_0=+0.08$ F.

It is perhaps worth noting that recently Pauli *et al.*[29] compared the π^+ angular distributions from π^+ scattering on deuterium with the elementary π^+p and π^-p angular distribution. The experiment covered the same c.m. energy region as the present one and excellent agreement of the π^+-deuterium results with the π-nucleon data was observed.

IV. THE $I=0$ PHASE SHIFTS

Again, different methods of analysis were used at 230 MeV/c and at the higher momenta. At the higher momenta, charge exchange and elastic plus inelastic scattering combined were fitted to Eqs. (7), (8), and (9). The data at each momentum were treated separately (the difference between 377 and 350 MeV/c was disregarded) and, as indicated, plane waves were used in the form factors for the outgoing nucleons. The scattering in the $I=1$ state was assumed to be purely *s* wave and the phase shift was taken from Ref. 1. The data were fitted using only an *s*-wave phase shift in $I=0$, then *s* and *p* waves and finally *s*, *p*, and *d* waves. Best fits are shown in Figs. 10–12 along with the data. The phase-shift results for *sp* and *spd* fits are also given in Tables IV and V, respectively. The *s* wave only solution had χ^2 probabilities $<1\%$ at all momenta and can be ruled out. The pairs of solutions at each momentum correspond to the Fermi-Yang ambiguity; the Minami ambiguity is absent because the *s*-wave phase shift in $I=1$ is fixed. The errors in Tables IV and V are given by $E_{ii}^{1/2}$ and the correlation coefficients C_{ij} by $E_{ij}/(E_{ii}E_{jj})^{1/2}$, where $(E^{-1})_{ij}=\frac{1}{2}(\partial^2\chi^2/\partial\delta_i\partial\delta_j)$ and χ^2 has the usual meaning. The correlation coefficients constrain the phase shifts more than the diagonal errors would suggest.

The momentum dependence of the phase shifts is illustrated in Figs. 13 and 14. The variation with momentum appears rational. The *d*-wave phase shifts do not scatter at random as might be expected if they were merely parameters used to improve the fit. Their consistency suggests either a real need for *d* waves or perhaps some persisting defect of the model. However,

[29] E. Pauli, A. Muller, R. Barloutaud, L. Cardin, J. Meyer, M. Beneventano, G. Gialanella, L. Paoluzi, and R. R. Finzi, Proceedings of the Siena Conference on Elementary Particles, 1963 (to be published).

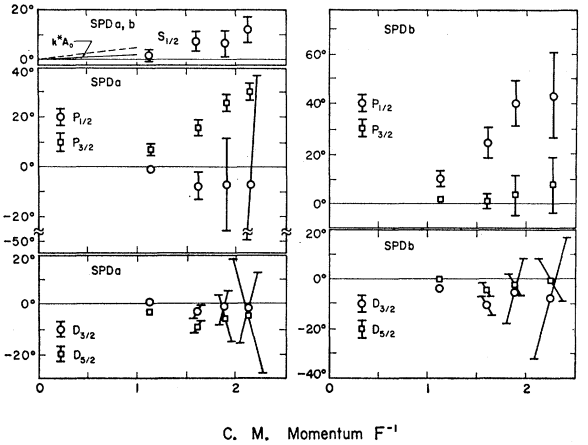

FIG. 14. The $I=0$ phase shifts of Table V plotted versus momentum. The a and b solutions are the Fermi-Yang ambiguity. The low-energy behavior of the s wave, as specified by the $I=0$ scattering length A_0, is also shown. The solid line refers to $A_0=+0.04$ F, the dotted line to $A_0=+0.08$ F.

as may be seen in Table V, even d waves do not secure a good fit at 377 MeV/c.

Because of the wide momentum spread of the incident beam shown in Fig. 1, the analysis of the 230-MeV/c data had to be carried out in a manner designed to circumvent the necessity to assign a k^* value to each event. Fortunately, Figs. 13 and 14 suggest that, for momenta below 230 MeV/c ($k^*<0.75$ F^{-1}), the phase shifts of the higher partial waves are very small. For this momentum range the zero-range approximation should be valid such that

$$\sin\delta_{T0}^{1/2}\approx k^* A_T. \tag{19}$$

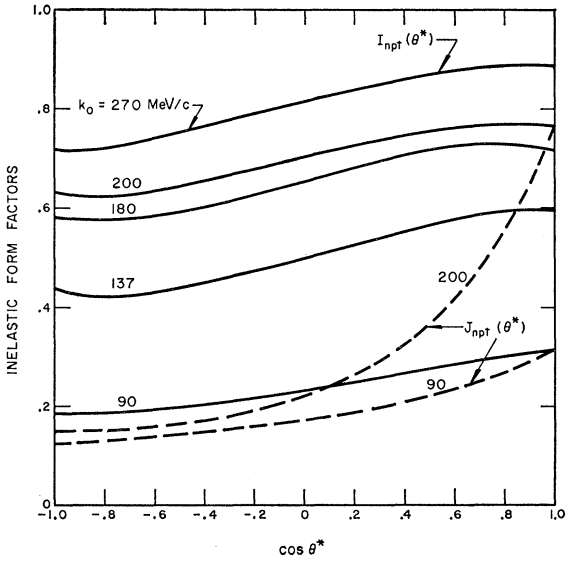

FIG. 15. The form factors I_{npt} and J_{npt} in the low-momentum region.

TABLE V. SPD solutions to phase-shift analysis. Subscripts 1, 2, 3, 4, 5 correspond to $\delta_{00}^{1/2}$, $\delta_{01}^{1/2}$, $\delta_{01}^{3/2}$, $\delta_{02}^{3/2}$, $\delta_{02}^{5/2}$.

k_0 MeV/c	$\delta_{10}^{1/2}$ deg.	$\delta_{00}^{1/2}$ deg.	$\delta_{01}^{1/2}$ deg.	$\delta_{01}^{3/2}$ deg.	$\delta_{02}^{3/2}$ deg.	$\delta_{02}^{5/2}$ deg.	Correlation coefficients C_{12}	C_{13}	C_{14}	C_{15}	C_{23}	C_{24}	C_{25}	C_{34}	C_{35}	C_{45}	χ^2	No. of const.	$P(\chi^2)$
350		2±2	−1±2	7±2	1±1	−3±1													
	−20.0						0.3	−0.8	−0.3	0.5	−0.5	0.1	−0.3	0.1	−0.4	−0.4	19.3	5	<0.01
(1.12 F^{-1})			10±4	2±1	−4±2	0±1	−0.8	−0.2	0.5	−0.2	−0.1	−0.3	0.1	−0.5	0.1	−0.3			
530		8±4	−8±6	16±4	−3±4	−9±3													
	−29.4						0.2	−0.8	0.6	−0.3	−0.3	0.4	−0.8	−0.6	0.3	−0.5	3.4	5	0.60
(1.60 F^{-1})			24±6	0±3	−11±4	−4±3	−0.7	−0.2	−0.3	0.5	−0.3	0.6	−0.6	−0.6	−0.0	−0.5			
642		6±6	−7±19	26±4	−1±7	−6±11													
	−36.2						0.6	−0.8	0.8	−0.7	−0.6	0.9	−1.0	−0.8	0.7	−0.9	3.6	2	0.16
(1.88 F^{-1})			40±10	3±9	−5±14	−2±4	−0.7	0.3	−0.6	0.7	−0.8	0.9	−0.8	−0.9	0.6	−0.8			
812		12±6	−7±44	30±4	−1±15	−4±24													
	−47.0						0.4	−0.6	0.7	−0.5	0.1	0.9	−1.0	−0.2	0.0	−1.0	0.4	2	0.80
(2.26 F^{-1})			43±17	8±12	−8±25	−1±9	0.3	−0.6	0.4	−0.2	−0.8	1.0	−0.9	−0.9	−0.7	−0.9			

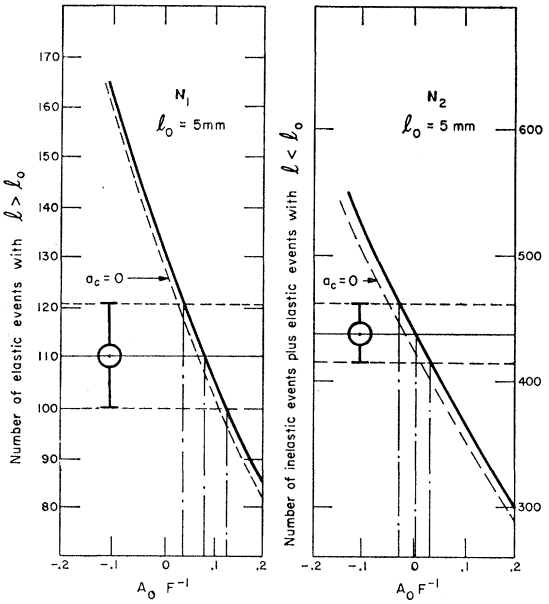

FIG. 16. The calculated and observed number of elastic scatters with recoil length larger than 5 mm and the calculated and observed number of all inelastic scatters and elastic scatters with recoil length smaller than 5 mm plotted versus $I=0$ scattering length. The solid line was calculated assuming a stationary nucleon in the Coulomb scattering amplitude.

As shown in Ref. 1, $A_1=-0.31\pm0.01$ F. The 230-MeV/c data may then be used to estimate A_0. With approximation (19), Eqs. (8) and (9) become

$$d\sigma^{\mathrm{IN}}/d\Omega^*\approx\{|A_1+a_c|^2+|A_1+A_0|^2/4\}I_{npt} +\mathrm{Re}\{(A_1+a_c)^*(A_1+A_0)\}J_{npt}, \quad (20)$$

$$d\sigma^{\mathrm{EL}}/d\Omega^*\approx\{|(A_1+a_c)+(A_1+A_0)/2|^2\}D. \quad (21)$$

In the low-momentum region, the form factor D, shown in Fig. 7, and I_{npt} and J_{npt}, shown in Fig. 15, vary rapidly with incident momentum. However, it is possible to integrate (20) and (21) with limits set such as to yield the expected numbers of elastic and inelastic events given in Table I once the incident beam momentum spectrum is given. The results of the calculation are shown in Fig. 16 for $l_0=0.5$ cm; A_0 is taken as variable. Both $a_c=0$ and a_c calculated for a target nucleon *at rest* are shown. The experimentally observed numbers are indicated. The A_0 estimate obtained using only elastic events, and A_0 obtained using the inelastic ones are in accord. The best estimate, taking into account all correlations, is $A_0=+0.04\pm0.04$ F. The A_0 estimate is insensitive to the choice of l_0; $l_0=1.2$ cm leads to the same value of A_0. The $\delta_{00}{}^{1/2}$ phase shift near zero momentum, based on this scattering length, is shown in Figs. 13 and 14 and appears to be consistent with the $\delta_{00}{}^{1/2}$ phase-shift determination at 377 MeV/c. Using $A_0=+0.04\pm0.04$ F and taking into account the K^+n-K^0p mass difference, one predicts a charge-exchange cross section of 1.2 ± 0.4 mb, in good agreement with the directly measured value[14] of $1.0_{-0.3}{}^{+0.4}$ mb.

V. CONCLUSIONS

The conclusions of this investigation may be stated briefly as follows:

(1) The phase shifts determined in this work using the plane-wave approximation for the outgoing nucleons are consistent with the phase shifts computed using the closure approximation.[14] Apart from a difference in sign of $\delta_{00}{}^{1/2}$ which is not understood, the phase shifts also seem to be in accord with those calculated in Ref. 18.

(2) In contrast to the A_1 scattering length of -0.31 ± 0.01 F, the A_0 scattering length is much smaller, $+0.04\pm0.04$ F being the best estimate of this work.

(3) At the present level of experimental precision, the final-state interaction between the nucleons may be neglected.

(4) Several "fine points" neglected by the impulse approximation, such as the inequality of $\cos\theta^{*\prime}$ and $\cos\theta^*$, the discrepancy between $k_{\mathrm{out}}{}^*$ and $k_{\mathrm{in}}{}^*$ and the D state of the deuteron constitute an error of 5 to 10% each. If the precision of the experiments is improved, it will be difficult to disregard these effects. It thus seems preferable to continue the studies of the $I=0$ interaction using K_2 beams colliding with protons.

ACKNOWLEDGMENTS

The authors wish to express their gratitude to Professor L. W. Alvarez for making the 15-in. bubble chamber available to them and for his support while this experiment was in progress. The important contributions of Professor W. Chinowsky and Dr. T. F. Stubbs, Dr. W. Lee, and Dr. T. O'Halloran during earlier phases of this work are gratefully acknowledged. The authors benefited greatly from discussions with Professor N. Byers concerning the theoretical aspects of the deuteron problems. The help of Dr. E. J. Lofgren and the Bevatron staff were greatly appreciated. We wish to thank R. Watt, G. Eckman, and the bubble chamber crews for their cooperation and the efficient running of the chamber. Last, but not least, our thanks to our scanning staffs at LRL and UCLA. Without their patient effort this work would not have been possible.

APPENDIX

For an incident nucleon state Ψ_D described by the Hulthèn wave function (15) and an outgoing nucleon state Ψ_P described plane waves, Eqs. (11) and (12)

may be integrated[23] and yield

$$F_0(Q,P)=4N^2\Bigg\{\frac{2}{[\alpha^2+(P+Q)^2][\alpha^2+(P-Q)^2]}+\frac{2}{[\beta^2+(P+Q)^2][\beta^2+(P-Q)^2]}-\frac{1}{PQ(\beta^2-\alpha^2)}\times\ln\frac{[\alpha^2+(P+Q)^2][\beta^2+(P-Q)^2]}{[\alpha^2+(P-Q)^2][\beta^2+(P+Q)^2]}\Bigg\},$$

$$G_0(Q,P)=\frac{4N^2-(\beta^2\alpha^2)}{2PQ[\alpha^2+\beta^2+2(P^2+Q^2)]}\times\Bigg\{\frac{1}{\alpha^2+P^2+Q^2}\ln\frac{[\alpha^2+(P+Q)^2]}{[\alpha^2+(P-Q)^2]}-\frac{1}{\beta^2+P^2+Q^2}\ln\frac{[\beta^2+(P+Q)^2]}{[\beta^2+(P-Q)^2]}\Bigg\}.$$

The integration of (14) using the Hulthèn function gives

$$H_2(Q)=\frac{\alpha\beta(\alpha+\beta)}{(\beta-\alpha)^2}\frac{2}{Q}\left[\tan^{-1}\frac{Q}{2\alpha}+\tan^{-1}\frac{Q}{2\beta}-2\tan^{-1}\frac{Q}{\alpha+\beta}\right].$$

PHYSICAL REVIEW VOLUME 134, NUMBER 5B 8 JUNE 1964

Bound States and Elementary Particles in the Limit $Z_3=0$†

M. L. WHIPPMAN AND I. S. GERSTEIN
Department of Physics, University of Pennsylvania, Philadelphia, Pennsylvania
(Received 27 January 1964)

The limit $Z_3=0$ is studied in the Zachariasen model using dispersion theory techniques. The connection between bound states and elementary particles is demonstrated in this limit and it is shown how Castillejo-Dalitz-Dyson ambiguities are removed.

I. INTRODUCTION

THERE has recently been a great deal of interest in studying field theories in the limit of vanishing renormalization constants.[1–3] Various authors have speculated that in this limit an "elementary particle" can be regarded as a bound state. Vaughn, Aaron, and Amado[4] have discussed the equivalence of the Lee model and potential theory in this limit. Rockmore, and Dowker and Paton[5] considered this problem in the context of the unsubtracted bootstrap model. A convenient model for studying this limit is that proposed by Zachariasen, in which the wave function renormalization can be determined explicitly and is finite. A special case of this theory in which there is no contact interaction has been studied by Acharya[6] and Dowker.[7] Dowker[8] has also discussed a more general case restricting himself to two dimensions and using perturbation theory.

Since the limit $Z_3=0$ is a highly singular one, it is advantageous to have explicit solutions for the quantities of interest and for this reason we shall confine our attention to the Zachariasen model.[9] The comparative simplicity of this theory allows us to see clearly the nature of the difficulties. Our work differs from that of Refs. 6, 7, and 8 in that we consider a wider class of solutions and obtain all our results in terms of finite physical quantities using dispersion theory techniques.

Our results may also be obtained from renormalized perturbation theory although we feel that results stated in terms of unrenormalized coupling constants, masses, etc., tend to be physically misleading.

In Sec. II we present a new dispersion theoretic method for solving the Zachariasen model based on the properties of the vertex function, rather than the denominator function. In Sec. II we exhibit and discuss several apparently different scattering solutions. We also consider the $Z_3=0$ limit of these solutions, and show their equivalence to a bound-state theory. Finally, in an Appendix we discuss a solution which clearly indicates the singular nature of the $Z_3=0$ limit.

II. PROPERTIES OF THE VERTEX AND CALCULATION OF Z_3

The Zachariasen model deals with the interaction of a scalar boson B (with a distinct antiparticle $\bar{B}$) and

† Supported by the U. S. Atomic Energy Commission.
[1] A. Salam, Nuovo Cimento **25**, 224 (1960); A. Salam, Phys. Rev. **130**, 1287 (1963).
[2] S. Weinberg, Phys. Rev. **130**, 776 (1963).
[3] R. Amado, Phys. Rev. **132**, 485 (1963).
[4] M. T. Vaughn, R. Aaron, and R. D. Amado, Phys. Rev. **124**, 1258 (1961).
[5] R. M. Rockmore, Phys. Rev. **132**, 878 (1963); J. S. Dowker and J. E. Paton, Nuovo Cimento **30**, 450 (1963).
[6] R. Acharya, Nuovo Cimento **24**, 870 (1962).
[7] J. S. Dowker, Nuovo Cimento **25**, 1135 (1962).
[8] J. S. Dowker, Nuovo Cimento **29**, 551 (1963).
[9] F. Zachariasen, Phys. Rev. **121**, 1851 (1961).